Stratigraphic and Structural Relations in Trench Exposures and Geomorphology at the Big Burn, Lily Lake, and Lester Ranch Sites, Bear River Fault Zone, Utah and Wyoming

By Suzanne Hecker, Christopher B. DuRoss, David P. Schwartz, Francesca R. Cinti, Riccardo Civico, William R. Lund, Adam I. Hiscock, Michael W. West, Tarka Wilcox, and Alivia R. Stoller

2019

U.S. Department of the Interior
U.S. Geological Survey

Cover. Photograph to the north along a west-facing fault scarp 4.5 kilometers south-southeast of the Lester Ranch trench site (lat 41.049° N., long 110.798° W.). Formation of the scarp caused blockage of an ephemeral stream that flowed to the northeast, resulting in ponding of water against the scarp (center of photograph). The continuation of the stream channel above the fault is preserved as a swale that intersects the crest of the scarp. Photograph by David P. Schwartz, July 2012.

Contents

Figure

Table

Introduction

This report provides trench photomosaics, logs and related site information (sheets 1–3), age data (appendix 1), and earthquake event evidence (table 1) from three paleoseismic trench sites on the Bear River Fault Zone. Our motivation for studying the Bear River Fault Zone—a nascent normal fault in the Rocky Mountains east of the Basin and Range physiographic province (fig. 1)—is twofold: (1) the intriguing conclusion from previous work that the neotectonic history of the fault may have begun in the middle to late Holocene and consists of only two surface-rupturing earthquakes (West, 1993, 1994) and (2) the question of whether large scarps (>10 meters [m] in height) observed along the fault represent net tectonic displacement, which, given a two-event history, would put the displacements among the largest in the Basin and Range region (Hecker and others, 2010). In presenting our trench and initial geomorphic interpretations, this report lays the groundwork for further exploration of these issues.

The surface trace of the west-dipping Bear River Fault Zone is ~44 kilometers (km) long, extending from the north flank of the Uinta Mountains (Utah) to 20 km east-southeast of Evanston, Wyoming, and comprises synthetic (down to the west) and antithetic scarps across a zone as much as 7.5 km wide (fig. 1). Two of our trench sites, Big Burn and Lily Lake, are located ~10 km from the south end of the fault on the main west-facing scarp and on a large antithetic scarp, respectively (fig. 1). The antithetic scarp, obscured by forest canopy, was unknown prior to this study. An airborne light detection and ranging (lidar) dataset with an average pulse density of 1.24 pulses per square meter (pulse/m^2) made available to us by the U.S. Forest Service allowed more detailed mapping of the fault's south end. The third site, Lester Ranch, is located on a prominent west-facing scarp in a section of right-stepping en echelon strands, ~11 km from the north end of the mapped fault in Wyoming (fig. 1). The southern sites are within glacial terrain on deposits mapped by Bryant (2010) as till (at Big Burn) and outwash (at Lily Lake) related to the late Pleistocene Pinedale glaciation. The Lester Ranch site is located on Pleistocene alluvial deposits that overlie a pediment cut on bedrock consisting of the Eocene Wasatch Formation (Dover and M'Gonigle, 1993; Reheis, 2005). Big Burn and Lester Ranch were two of several sites trenched in the early 1980s and the original Lester Ranch trench provided the clearest evidence of a two-event history on the fault (West, 1993, 1994).

Methods

We excavated paleoseismic trenches across the Bear River Fault Zone at the Big Burn site in 2009, Lily Lake (antithetic fault) in 2013, and Lester Ranch in 2016. Field crews spent 5 to 8 days at each site and our field work followed established paleoseismic trenching practice (for example, McCalpin, 2009a). The trenches were excavated perpendicular to the scarps with rubber-tired backhoes, with vertical south wall exposures, and sloped and benched north wall exposures
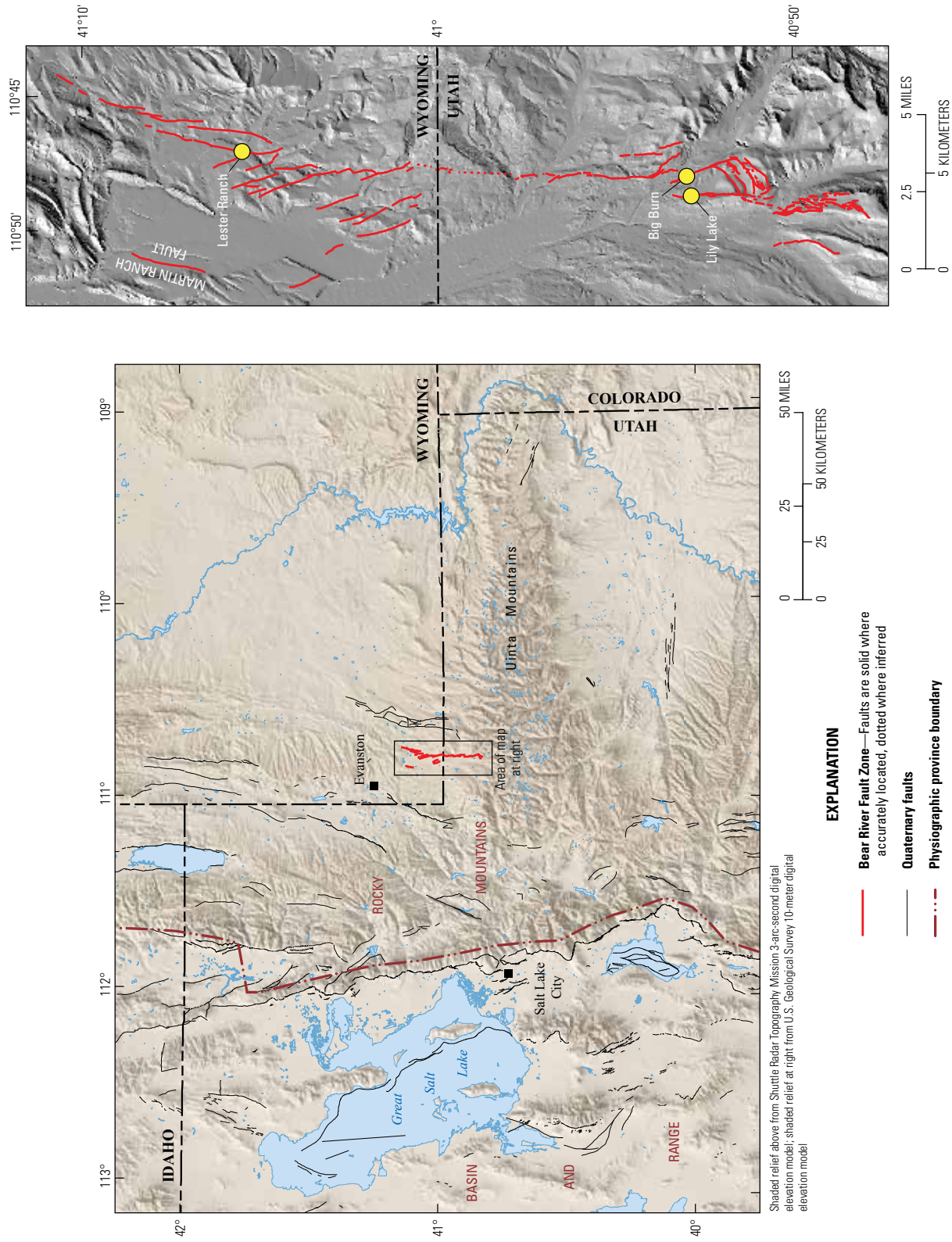
for stability. Because of the exceptional size of the scarp at Big Burn (~17 m high; sheet 1), we were only able to excavate into the base (lower 5 m) of the scarp and across an adjacent closed depression. The vertical south wall of each trench was gridded at 1-m spacing (2 m horizontal and 1 m vertical spacing at Big Burn) using a measuring tape and level. We then photographed the wall and created a composite image (photomosaic), which was used as a base map to log the exposed stratigraphy and structures. For the Big Burn and Lily Lake trenches, we created the photomosaics by manually rubber-sheeting photographs of each string-gridded rectangle onto a rectangular grid. For the Lester Ranch trench, we used structure-from-motion photogrammetry with overlapping photographs (>50 percent) and with marked grid intersections (but no string) to create a seamless, high-resolution photomosaic of the wall (see Reitman and others, 2015, for an example of the methodology). We sampled detrital charcoal, organic fragments, and (or) sediment containing organic material for radiocarbon dating and sampled fine to medium sand for optically stimulated luminescence (OSL) dating at strategic locations in the trenches to establish chronological constraints on the evidence of paleoseismic events.

Site Stratigraphy, Structure, and Geomorphology

Big Burn Trench

The Big Burn trench, located at the base of the main, west-facing scarp in Utah, exposed tilted and faulted glacial deposits overlain by a younger 1.5-m-thick sequence of depression-fill deposits and colluvium (sheet 1). The closed depression at the base of the scarp was originally thought to be caused by antithetic faulting, but lidar imagery (from data obtained from the U.S. Forest Service in 2012) shows that the depression is related to the original undulating glacial topography. This observation is consistent with the absence of measurable displacement on mapped fractures west of the main scarp (sheet 1).

The infill and colluvial sequence at the base of the scarp at the Big Burn site is much thinner than would be expected for such a large scarp produced by surface faulting. Although the trench did not reach as high as the middle of the scarp where the main fault plane would be expected (McCalpin, 2009b), scarp degradation models for morphologically simple scarps predict that the maximum thickness of colluvium deposited on a nearly horizontal surface is approximately 50 percent of the scarp height (McCalpin, 2009b), which would mean a colluvial thickness of ~8.5 m for the simple (smooth-faced) ~17-m-high scarp at the Big Burn trench (sheet 1). A key observation is that an illuvial soil horizon (a Btk horizon characterized by accumulation of silicate clays and calcium carbonate) mapped in the glacial till lies in a slope-parallel orientation beneath the lower portion of the scarp (beneath thin hillslope colluvial units 1ch and 2ch and truncated by scarp colluvial unit 3cs; horizontal meter 2 to 6, sheet 1). We interpret this to indicate that

Figure 1. Shaded-relief map of the Bear River Fault Zone in relation to other Quaternary faults and the eastern boundary of the Basin and Range physiographic province. Fault locations are from the Quaternary Fault and Fold Database of the United States (QFFD; U.S. Geological Survey and Utah Geological Survey, 2016). Map inset shows the location of our paleoseismic trench sites on the Bear River Fault Zone. Fault trace is modified from QFFD using light detection and ranging (lidar) shaded-relief imagery in Utah south of ~40°55'30" N (from data provided by U.S. Forest Service) and 1994–2017 Google Earth imagery farther north in Utah and Wyoming. The 4-kilometer-long down-to-the-west Martin Ranch Fault is included here as part of the Bear River Fault Zone.

the ground surface here was tilted forward and bent, or folded, rather than being substantially faulted (sheet 1; see discussion of monoclinal scarps in McCalpin, 2009b). A monoclinal-folding origin for the scarp, whereby material was not exposed on a steep free face, would account for the paucity of colluvium and also for the unusually narrow (undegraded) scarp crest and base as well as the planar midsection (sheet 1). Folding of the land surface also explains the apparent preservation of hummocky glacial morphology across the face of the scarp, as identified on bare-earth shaded-relief imagery (sheet 1).

Lily Lake South Trench

The Lily Lake south trench, located 1 km west of the Big Burn site on a large east-facing scarp, also shows evidence for monoclinal folding of glacial deposits (sheet 2). This antithetic strand of the Bear River Fault Zone cuts across a west-facing valley-side hillslope, forming an uphill-facing scarp expressed as a prominent bench (sheet 2). We excavated two trenches across this bench, the northern of which appeared to be less informative, as it exposed a stack of massive mass-wasting deposits with poorly expressed faults, and thus was not logged. The south trench was sited across a geomorphic low where sediment has collected, forming a small flat. Glaciofluvial deposits (unit 3gf) exposed beneath the outer edge of the topographic bench are gently folded across the hinge of an east-facing monocline (near meter 14, sheet 2). These units are also cut by minor down-to-the-east faults (near meter 12). Mass-wasting and alluvial deposits (units 2tf, 2tfm, and 2tfa; meter 5 to 13) infill the structural trough produced by the monoclinal folding and related faulting and are, in turn, tilted eastward on the limb of the growing monocline. Ponded sediments infill the depression created by folding of the trough-fill sequence (unit 1df, meter 2 to 7), and these deposits have been slightly faulted as well. Folding documented in the trench is responsible for most (~5.5 m) of the ~6.5 m of vertical separation measured at the site (sheet 2).

Lester Ranch Trench

In contrast to the sites on glacial deposits, where surface displacement is accommodated mainly by folding, the Bear River Fault Zone ruptures through to the ground surface at the Lester Ranch site, which lies on Eocene Wasatch Formation (Tw) bedrock covered by only a thin veneer of deposits (sheet 3). The main fault zone exposed in the Lester Ranch trench consists of several fault strands (F1–F3) in a 6-m-wide zone that has accommodated about 6 m of down-to-the-west vertical separation of Pleistocene pediment alluvium (4al, sheet 3). Bedrock stratigraphy exposed across F1 is not readily correlatable, and the easternmost strand of F2 appears to terminate at the base of the Pleistocene alluvium, suggesting an older history of faulting. The alluvium and bedrock beneath the fault scarp are overlain by elongate, wedge-shaped deposits

of colluvium (units 2csw, 2csd, and 3cs). Soils or subtle weathering zones mark the top of the alluvium and the top of the lower colluvium. An apparent debris slide in the upper part of the colluvial section (unit 1ds), suspected of being seismically triggered, is evidenced by (1) a thickening of deposits that corresponds to the location of an irregular, gently sloping topographic bench (meter 16 to 22.5, sheet 3), which extends along the base of the scarp for ~80 m, (2) a concave-up contact within the deposits (the slide plane), expressed as differential relief and a discontinuous light-colored zone partly bleached of organics, and (3) a small scarp (near meter 13) and surface depression upslope of the slide mass (meter 13 to 14.5) that we interpret as the head scarp and upper part of the source area. The head scarp is underlain by minor distributed faulting and may be tectonic in part. An alternative explanation for the bench, supported by its linearity and extent, but controverted by its side-sloping morphology, is that it is a bladed road created along the base of the fault scarp. The longstanding ranch owner was unaware of any earthmoving activities at that location, however. The bench is visible on 1:20,000-scale aerial photographs from 1960 (U.S. Department of Agriculture Farm Service Agency, 1960).

Earthquake Event Evidence

In table 1, we present evidence of ground-deforming earthquakes observed in the trenches (sheets 1–3) and we evaluate the quality of each piece of evidence, similar to the ranking system developed by Scharer and others (2007) for strike-slip faults. We use a three-tiered scale of low, moderate, and high to reflect the degree of certainty that the observed or inferred deformation was produced by an earthquake.

We find evidence consistent with a record of three earthquakes at each site, although the strength and number of observations vary between events and trenches (table 1). Evidence for three earthquake events is strong at Lily Lake, whereas evidence for the youngest event (E1) is fairly weak at both Big Burn and Lester Ranch. Inspection of the available radiocarbon and OSL ages (sheets 1–3; appendix 1) and comparison of the Lester Ranch trench log (sheet 3) with the log from the 1983 trench exposure indicate that the two older earthquake events (E2 and E3) likely correspond to the middle to late Holocene ruptures identified by West (1993, 1994). The youngest event (E1), which was not recognized prior to our study, likely occurred within the last several hundred years, as indicated by ages of macrofloral remains from deposits that predate the earthquake (table 1.2).

Elements of this study yet to be completed include (1) documenting off-fault evidence for E1, (2) analyzing earthquake event ages, (3) estimating cumulative and event displacements on the fault, and (4) considering the factors responsible for clustering of large earthquakes on the Bear River Fault Zone and perhaps on other faults in comparable settings (Hecker and Schwartz, 2018).

Table 1. Location and quality of earthquake event evidence from Big Burn (BB), Lily Lake south (LL), and Lester Ranch (LR) paleoseismic trenches (sheets 1, 2, and 3, respectively), Bear River Fault Zone, Utah and Wyoming.

Trench–Event	Event evidence	Quality rank	Description and interpretation of event evidence
BB–E3	Base of depression-fill deposits (unit 3df, meter 7 to ~18?)	Moderate	Initiation of sedimentation in closed basin adjacent to scarp likely triggered by initial post-glacial deformation
BB–E3	Scarp colluvium (unit 3cs, meter 6 to 8)	Moderate	Wedge-shaped deposit truncates the Btk soil horizon developed in glacial deposits and grades laterally into depression fill; original geometry of wedge and associated scarp is somewhat ambiguous
BB–E3	Upward fault terminations (meter 6 to 7)	Low	Terminations at base of units 3df and 3cs may be apparent only; material properties allow for concealment of minor faults
BB–E2	Hillslope colluvium (unit 2ch, meter 2 to 9)	Moderate	Discrete coarse-grained slope deposit buries older colluvium (unit 3cs) and extends farther downslope, suggesting a shift in the toe of the slope owing to growth of the scarp; sediment mobilization inferred to be triggered by folding event (blind causative fault) that steepened and broadened the flexure and possibly by minor fault rupture higher on the scarp (though not evidenced in the scarp's morphology)
BB–E2	Top of depression infill (unit 3df) that buries toe of unit 2ch colluvium (meter 9)	Low	Slope colluvium is buried by continued or renewed ponding of sediment in the depression, consistent with deformation-induced sedimentation
BB–E1	Hillslope colluvium (unit 1ch, meter 2 to 10)	Low	Discrete, but thin, slope deposit that buries older colluvium (unit 2ch) and extends farther downslope, suggesting a shift in the toe of the slope owing to growth of the scarp; sediment mobilization inferred to be triggered by folding event (blind causative fault) that steepened and broadened the flexure; however, matrix-supported nature of deposit allows for an alternative sediment-mobilization mechanism (for example, a storm event)
LL–E3	Unconformable relation between top of folded glacial deposits (unit 3gf) and overlying trough-fill deposits (units 2tf, 2tfm and 2tfa, meter 10 to 16)	High	Alluvial and mass-wasting deposits accumulated in a broad hillside trough (uphill-facing scarp) created by folding and eastward tilting of glacial deposits that underlie the hillside
LL–E2	Unconformable relation between top of folded trough-fill deposits (unit 2tfm) and overlying depression-fill deposits (unit 1df, meter 2 to 7)	High	Predominately fine-grained sediments accumulated in depression created by folding and eastward tilting of trough-fill sequence (rejuvenating the buried uphill-facing fold scarp); depression-fill unit thickens over fold hinge and pinches out against fold limb
LL–E1	Faulting of post-E2 depression-fill deposit (unit 1df) and ground surface (meter 5 to 6)	High	Displacement of unit 1df and overlying top soil forms a small (~15-centimeter-high) scarp on the forest floor
LR–E3	Scarp colluvium (unit 3cs, meter 14 to ~19)	Moderate	Faulted and truncated colluvial deposit that buries what appears to be the pre-faulting ground surface (deposit interpreted to be unit 4al, with remnant soil horizon, between faults F2 and F3), recording the first scarp-forming event; deposit thickens in small graben at meter 15
LR–E3	Upward termination of fault F3 (meter 17 to 17.5)	Moderate	F3 appears to thrust a block of unit 4al onto the event ground surface (top of A horizon formed in unit 4al); however, position of ground surface is uncertain and properties of overlying material (unit 3cs) allow for upward continuation of minor faulting

Table 1. Location and quality of earthquake event evidence from Big Burn (BB), Lily Lake south (LL), and Lester Ranch (LR) paleoseismic trenches (sheets 1, 2, and 3, respectively), Bear River Fault Zone, Utah and Wyoming.—Continued.

Trench–Event	Event evidence	Quality rank	Description and interpretation of event evidence
LR–E2	Scarp colluvium (units 2csw and 2csd, meter 9.5 to ~19)	High	Lower coarser grained facies (unit 2csd, meter 14 to 18) is distinct from underlying unit 3cs colluvium (and separated from it by a subtle soil) and contains blocks of material suspected to be derived from an upthrown unpreserved portion of unit 3cs east of F2; the upper deposit (unit 2csw), interpreted as mainly wash-facies colluvium (with coarser grained deposits upslope from F1 at meter 11), is unusually laterally extensive and its genesis is not entirely clear
LR–E1	Fractures mapped in E2 colluvium (meter 10 to 16); open fractures in unit 4al (meter 3 and 7)	Low	Distributed fractures and minor faults appear to extend to, or close to, the ground surface; unfilled voids along fractures in unit 4al suggest recency of faulting
LR–E1	Debris slide off of scarp (meter 13 to 22.5)	Low	Spatial association with fault zone suggests apparent slope failure was triggered by ground shaking and possibly surface rupture; however, an artificial origin for the topographic bench formed by the deposit (unit 1ds) cannot be precluded

Acknowledgments

References Cited

Bryant, B., 2010, Geologic map of the east half of the Salt Lake City 1° x 2° quadrangle (Duchesne and Kings Peak 30′×60′ quadrangles), Duchesne, Summit, and Wasatch Counties, Utah, and Uinta County, Wyoming (digitized and modified from U.S. Geological Survey Miscellaneous Investigations Series Map I-1997, published in 1992): Utah Geological Survey Miscellaneous Publication 10-1DM, GIS data, 2 plates, scale 1:125,000.

Dover, J.H., and M'Gonigle, J.W., 1993, Geologic map of the Evanston 30′×60′ quadrangle, Uinta and Sweetwater Counties, Wyoming: U.S. Geological Survey Miscellaneous Investigations Series Map I-2168, scale 1:100,000.

Hecker, S., Dawson, T.E., and Schwartz, D.P., 2010, Normal-faulting slip maxima and stress-drop variability—A geological perspective: Bulletin of the Seismological Society of America, v. 100, no. 6, p. 3130–3147, https://dx.doi.org/10.1785/0120090356.

Hecker, S., and Schwartz, D.P., 2018, Behavior of a new normal fault in the Rocky Mountains—Implications for continental intraplate earthquakes [abs.]: Geological Society of America Abstracts with Programs, v. 50, no. 6, https://doi.org/10.1130/abs/2018AM-324944.

McCalpin, J.P., 2009a, Field techniques in paleoseismology—Terrestrial environments, chap. 2A of McCalpin, J.P., ed., Paleoseismology (2d ed.): International Geophysical Series, v. 95, p. 29–118.

McCalpin, J.P., 2009b, Paleoseismology in extensional tectonic environments, chap. 3 of McCalpin, J.P., ed., Paleoseismology (2d ed.): International Geophysical Series, v. 95, p. 171–269.

Prescott, J.R., and Hutton, J.T., 1994, Cosmic ray contributions to dose-rates for luminescence and ESR dating—Large depths and long-term time variations: Radiation Measurements, v. 23, no. 2/3, p. 497–500.

Reheis, M.C., 2005, Surficial geologic map of the upper Bear River and Bear Lake drainage basins, Idaho, Utah, and Wyoming: U.S. Geological Survey Scientific Investigations Map 2890, scale 1:50,000 and 1:150,000.

Reitman, N.G., Bennett, S.E.K., Gold, R.D., Briggs, R.W., and DuRoss, C.B., 2015, High-resolution trench photomosaics from image-based modeling—Workflow and error analysis: Bulletin of the Seismological Society of America, v. 105, no. 5, p. 2354–2366.

Scharer, K.M., Weldon, R.J., Fumal, T.E., and Biasi, G.P., 2007, Paleoearthquakes on the southern San Andreas Fault, Wrightwood, California, 3,000 to 1,500 B.C.—A new method for evaluating paleoseismic evidence and earthquake horizons: Bulletin of the Seismological Society of America, v. 97, p. 1054–1093, https://dx.doi.org/10.1785/0120060137.

Stuiver, M., and Pollach, H.A., 1977, Discussion—Reporting of ^{14}C data: Radiocarbon, v. 19, p. 355–363.

Stuiver, M., Reimer, P.J., and Reimer, R.W., 2017, CALIB 7.1 [WWW program] accessed May 3, 2017, at http://calib.org.

U.S. Department of Agriculture Farm Service Agency, 1960, Aerial photographs flown August 18, 1960: U.S. Department of Agriculture Aerial Photography Field Office photographs CVT-6AA-122 and 123, scale 1:20,000 [vertical black and white film].

U.S. Geological Survey and Utah Geological Survey, 2016, Quaternary fault and fold database for the United States: U.S. Geological Survey database, accessed October 6, 2016, at https://earthquake.usgs.gov/hazards/qfaults/.

West, M.W., 1993, Extensional reactivation of thrust faults accompanied by coseismic surface rupture, southwestern Wyoming and north-central Utah: Geological Society of America Bulletin, v. 105, p. 1137–1150.

West, M.W., 1994, Seismotectonics of north-central Utah and southwestern Wyoming in Paleoseismology of Utah, v. 4: Utah Geological Survey Special Study 82, 93 p.

Appendix 1

Table 1.1 Results of radiocarbon age dating of detrital charcoal from Big Burn (Bear) and Lily Lake south (LLS) trenches, Bear River Fault Zone, Utah; data collected at the Center for Accelerator Mass Spectrometry, Lawrence Livermore National Laboratory.

[‰, parts per thousand; yr B.P, years before present; cal. yr B.P., calibrated years before present]

Lab number (CAMS no.)[a]	Field number[b]	Report date	$\delta^{13}C$ (‰)[c]	^{14}C age (yr B.P.)[d]	Calibrated age (cal. yr B.P.)[e]
146537	Bear 4 (R-B4)	Mar. 14, 2010	−25	4,330 ± 35	4,970–4,840
146538	Bear 6 (R-B6)	Mar. 14, 2010	−25	2,495 ± 30	2,730–2,470
166517	LLS-S1*	June 23, 2014	−23.02	675 ± 30	680–560
166518	LLS-S2*	June 23, 2014	−24.04	860 ± 30	900–690
166519	LLS-S3*	June 23, 2014	−26.87	3,710 ± 30	4,150–3,980
166520	LLS-S4*	June 23, 2014	−25.01	3,095 ± 25	3,370–3,240
166521	LLS-S5*	June 23, 2014	−21.96	3,020 ± 30	3,320–3,080
166528	LLS-S6*	June 23, 2014	−25.2	905 ± 25	910–760
166522	LLS-S7*	June 23, 2014	−24.09	3,050 ± 30	3,350–3,180

[a] Laboratory identifier: CAMS, Center for Accelerator Mass Spectometry, Lawrence Livermore National Laboratory.

[b] Samples with an asterisk (*) were large enough for $\delta^{13}C$ aliquots to be taken.

[c] $\delta^{13}C$ values are the assumed values according to Stuiver and Polach (1977) when given without decimal places. Values measured for the material itself are given with decimal places.

[d] Reported in radiocarbon years before present (1950) using the Libby half-life of 5,568 years and following the conventions of Stuiver and Polach (1977). Error is one standard deviation (1σ) analytical uncertainty.

[e] 2σ calibrated age range rounded to nearest decade; calibration from CALIB 7.1 program (Stuiver and others, 2017).

Table 1.2 Results of radiocarbon dating of macrofloral remains from Lily Lake south (LLS) and Lester Ranch (LR) trenches, Bear River Fault Zone, Utah and Wyoming; data collected at the PaleoResearch Institute in Golden, Colorado.

[‰, parts per thousand; %, percent; AMS, accelerator mass spectrometry; yr B.P., years before present; cal. yr B.P., calibrated years before present]

Sample number	Sample identification	Report date	$\delta^{13}C$ (‰)[a]	AMS ^{14}C age (yr B.P.)[b]	Calibrated age (cal. yr B.P.)[c]
PRI-14-071-LLS9-1	*Pinus* cone scale, charred	January 2015	−23.6	244 ± 22	310–280 (73) 170–150 (25)
PRI-14-071-LLS9-2	*Pinus* cone scale, charred	January 2015	−24.3	369 ± 21	500–430 (63) 380–320 (36)
PRI-14-071-LLS9-3	*Pinus* needle, charred	January 2015	−25.7	387 ± 23	510–430 (79) 360–330 (20)
PRI-5610-LR-1	*Artemisia* and unidentified hardwood charcoal, incompletely charred	February 2017	−26.16	378 ± 22	500–430 (71) 380–320 (29)

[a] $\delta^{13}C$ values are measured by AMS during the ^{14}C measurement. The AMS $\delta^{13}C$ values are used for the ^{14}C calculation and should not be used for dietary or paleoenvironmental interpretations.

[b] Reported in radiocarbon years before present (1950) with one standard deviation (1σ) analytical uncertainty, corrected for $\delta^{13}C$.

[c] 2σ calibrated age range rounded to nearest decade; calibration from CALIB 7.1 program (Stuiver and others, 2017). Parenthetical probabilities of occurrence, in percent, reflect multimodal age distributions.

Table 1.3 Quartz optically stimulated luminescence (OSL) data and ages for Lily Lake south and Big Burn trenches, Bear River Fault Zone, Utah, from the U.S. Geological Survey Luminescence Dating Laboratory in Denver, Colorado.

[%, percent; wt. %, weight percent; ppm, parts per million; Gy, grays; Gy/ka, grays per thousand years]

Field number	Water content (%)[a]	K (wt. %)[b]	U (ppm)[b]	Th (ppm)[b]	Cosmic dose (Gy/ka)[c]	Total dose rate (Gy/ka)	Equivalent dose (Gy)	n[d]	Scatter (%)[e]	Age (years)[f]
OSL-LLS1	1 (24)	2.30 ± 0.04	2.23 ± 0.20	13.3 ± 0.37	0.30 ± 0.01	3.82 ± 0.08	60.8 ± 3.83	3 (30)	43	15,910 ± 1,060
OSL-B1	0 (31)	2.55 ± 0.10	2.79 ± 0.26	12.5 ± 0.54	0.28 ± 0.01	4.05 ± 0.11	18.2 ± 0.52	9 (20)	41	4,500 ± 280
OSL-B2	0 (23)	2.37 ± 0.07	3.05 ± 0.22	11.3 ± 0.48	0.28 ± 0.01	3.94 ± 0.10	13.5 ± 0.44	7 (18)	43	3,430 ± 200
OSL-B3	0 (21)	2.77 ± 0.05	2.15 ± 0.19	11.3 ± 0.42	0.29 ± 0.01	4.13 ± 0.09	55.0 ± 1.68	8 (18)	31	13,310 ± 500
OSL-B4	0 (27)	2.02 ± 0.04	2.34 ± 0.17	10.8 ± 0.46	0.30 ± 0.01	3.40 ± 0.08	31.9 ± 0.78	14 (20)	39	9,390 ± 360

[a] Field moisture; figures in parentheses indicate the complete sample saturation percentage. Ages calculated using field moisture.

[b] Analyses obtained using high-resolution gamma spectrometry (Ge detector).

[c] Cosmic doses and attenuation with depth were calculated using the methods of Prescott and Hutton (1994).

[d] Number of replicated equivalent dose estimates used to calculate the equivalent dose. Figures in parentheses indicate total number of measurements included in calculating the represented equivalent dose and age using the minimum age model.

[e] Defined as "over-dispersion" of the equivalent dose values; obtained by dividing the average by the standard deviation. Values >25 percent are considered to be poorly bleached (or mixed) sediments.

[f] Age for fine-grained (180–250 microns) quartz. Exponential fit used on equivalent doses; reported errors are two standard deviations, ages and errors rounded to nearest decade.